12th IFAC International Symposium on
Advanced Control of Chemical Processes
July 14-17, 2024. Toronto, Canada

Dynamic Optimization of Chemical Looping Reforming Fixed Bed Reactor for Blue Hydrogen Production

Adrian R. Irhamna * **George M. Bollas** *

* *Department of Chemical and Biomolecular Engineering, University of Connecticut, Storrs, CT 06269 USA (e-mail: george.bollas@uconn.edu).*

Abstract:
Chemical-looping Reforming (CLR) offers a promising process option for Blue Hydrogen production. Fixed-bed CLR reactors are ideal for process intensification, but require an effective control strategy to maximize hydrogen production in a dynamic process that needs to satisfy constraints imposed by process safety concerns and concomitant target products. To realize this goal, we use dynamic modeling and optimization for the design and control of an optimal fixed-bed CLR reactor. The optimal control strategy in the CLR reactor not only enables autothermal operation but also efficiently manages the heat recovery from the exhaust gas for feed gas preheating. As a result, the reactor produces syngas with an H_2/CO ratio of 3 and generates stream of a high N_2 concentration ($> 98\%$) in each CLR cycle. Without hydrogen shift units, the reactor achieved a hydrogen yield efficiency of 62%.

Keywords: Chemical looping reforming, fixed-bed reactor, dynamic optimization, Blue Hydrogen, process control

1. INTRODUCTION

A recent report on global temperature trends [NASA (2023)] highlights the consistent temperature rise of 0.03°C per year in the past 30 years. The steady global temperature rise emphasizes the need to reduce greenhouse gas emissions. Moving away from carbon-based fuel sources is believed as the most effective approach for this goal [UN Climate Change (2023)]. Hydrogen emerged as a promising clean energy carrier since it contains no carbon and produces only water when oxidized. As a matter of fact, hydrogen has been pivotal as the main feedstock in fertilizer and petroleum refining industries for decades. A substantial surge in hydrogen demand, around three times the current level, is expected in 2050 due to this energy shift [IEA (2020)]. Despite its importance, hydrogen gas constitutes only around 0.6 ppm in our atmosphere. Approximately 95% of global hydrogen gas is produced from steam methane reforming (SMR) of fossil fuels, an established H_2 production technology that emits over 11 kg of CO_2 per kg of H_2 [IEA (2023)]. The main CO_2 emissions in SMR arise from the combustion of natural gas to generate heat for the process. At best, hydrogen produced through this method is often referred to as Grey Hydrogen, leading to the classification of hydrogen based on a color spectrum [Arcos and Santos (2023)].

Among the spectrum of hydrogen colors, Green and Blue hydrogen have emerged as the most mature and extensively researched options for decarbonizing hydrogen production [Newborough and Cooley (2020)]. Green Hydrogen symbolizes the ideal scenario for a complete departure from carbon-based energy sources. However, a substantial challenge remains: the cost of Green Hydrogen production is relatively high, approximately four times more expensive than traditional Grey Hydrogen [Bloomberg NEF (2020)]. On the other hand, Blue Hydrogen, though unable to entirely eliminate CO_2 emissions, proves to be a more cost-effective alternative to Green Hydrogen. The current price of Blue Hydrogen is around 1.7-2.6 USD/kg-H_2, roughly twice that of Grey Hydrogen [Bloomberg NEF (2020)]. This places Blue Hydrogen as a bridging technology toward zero-carbon alternatives. A recent study suggests that by 2050, with the implementation of carbon pricing and taxes, Blue Hydrogen is predicted to be the most economical option compared to Grey and Green Hydrogen [George et al. (2022)]. However, Blue Hydrogen faces scrutiny, especially concerning the practical implementation of carbon capture technology and the potential for fugitive methane emissions from upstream activities [Howarth and Jacobson (2022)].

Chemical-looping Reforming (CLR) has emerged as an alternative process for Blue Hydrogen production route, offering the potential for a smaller footprint and lower capital and operating cost [Arnaiz del Pozo and Cloete (2022)]. CLR operates in three different stages: Oxidation, Reduction, and Reforming, as illustrated in Figure 1. Each stage produces an exit stream with a high concentration of N_2, an exit stream with CO_2 and steam, and a third stream with a high concentration of syngas, specifically hydrogen. The CO_2-H_2O stream can be separated by a simple condenser unit before storing CO_2 to achieve the Blue Hydrogen concept. The heat required for the process is provided by the oxidation of oxygen carriers. Essentially, the CLR process intensifies the reformer, heat source, air

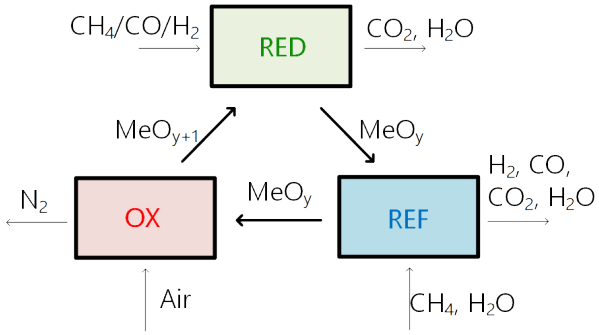

Fig. 1. Schematic description of typical Chemical-looping Reforming (CLR) process

separation, and CO_2 separation processes into a single operation. Furthermore, CLR has the potential to emit the least amount of CO_2 emissions compared to other Blue Hydrogen technologies. According to techno-economic studies [Nazir et al. (2021)], hydrogen production through CLR and CCS is estimated to result in emissions of less than than 0.8 kg-CO_2/kgH_2, which is 10 times smaller than that of Grey Hydrogen. Figure 1 illustrates the typical CLR process. The performance of CLR lies in the ability of oxygen carriers to undergo REDOX and catalytic reactions. The common oxygen carriers and catalysts for CLR include Ni, Fe, and Cu [Adanez et al. (2012)].

In this work, we focus on evaluating the performance of a CLR reactor for Blue Hydrogen production. We chose the fixed-bed reactor due to its operational simplicity, elimination of the need for solid separation, and its widespread use in reforming processes [Han et al. (2013, 2014)]. Our objective is to investigate an optimal control strategy by solving an optimization problem that maximizes hydrogen production, while meeting the requirements for potential for nearly pure N_2 production that can be used for ammonia synthesis. The general concept in this work, is to design multiple fixed bed reactors operating in parallel in order to process a continuous stream of fuel and air. From a design optimization perspective, it is more practical to optimize the operation of a single fixed bed CLR reactor and subsequently apply the optimal process to a series of identical reactors. This study concludes by discussing potential areas for improvement and challenges to enhance the performance of the reactor design and configuration.

2. CLR PROCESS DESCRIPTION

A fixed bed reactor is used to investigate and optimize CLR performance for Blue Hydrogen production. Achieving an optimal control scenario for this individual reactor is important since it will serve as a model for multiple reactors operating in parallel to ensure a continuous downstream. The reactor operates dynamically following three CLR stages: Oxidation (OX), Reduction (RED), and Reforming (REF). In OX, air oxidizes the oxygen carrier bed generating heat for the process. Under optimal conditions, OX is expected to produce a downstream gas with high N_2 concentration. OX concludes when the heat required for RED and REF is sufficient in the reactor bed. During RED, the feed comprises a low-concentration fuel diluted with CO_2 - for instance, off-gas from a purification unit, is used as reduction gas, for reducing oxygen carriers into an active metal catalyst. The stage switches to REF when a sufficient catalyst is available in the bed for the reforming process. In REF, methane and steam react to produce syngas (H_2 and CO) aided by a catalyst at high temperatures. The process switches back to OX, as more methane slips are detected in the product gas, completing one cycle of CLR.

3. MODELLING

3.1 Reactor Model

The CLR fixed bed reactor is simulated using a 1D heterogeneous dynamic model that accounts for mass and energy balance in both the solid and fluid phases within the reactor. The pressure drop across the reactor is calculated using the Ergun equation. The partial differential equations (PDEs) governing the fixed-bed reactor model are summarized in Table 1. The model incorporates the reaction kinetics of Ni-based oxygen carriers, which have been extensively developed and studied previously [Zhou et al. (2013, 2014); Nordness et al. (2016); Han et al. (2016a,b)]. The list of reactions used in the model is shown in Table 2, with the corresponding kinetic expressions provided in [Han and Bollas (2016)].

Table 1. Design equations for the fixed bed reactor model

Fluid phase

Mass Balance:

$$\epsilon_b \frac{\partial C_i}{\partial t} + \frac{\partial u C_i}{\partial z} = \epsilon_b \frac{\partial}{\partial z}\left(D_{\mathrm{ax},i} \frac{\partial C_i}{\partial z}\right) + k_{c,i} a_v \left(C_{c,i}\big|_{Rp} \quad C_i\right)$$

Energy Balance:

$$\epsilon_b C_{p,f} C_T \frac{\partial T}{\partial t} + C_{p,f} C_T \frac{\partial u T}{\partial z} = \epsilon_b \frac{\partial}{\partial z}\left(\lambda_{\mathrm{ax}} \frac{\partial T}{\partial z}\right) + h_f a_v \left(T_c\big|_{Rp} \quad T\right) + \frac{4U}{D_r}(T \quad T_w)$$

Momentum Balance:

$$\frac{dP}{dz} = \left(\frac{1-\epsilon_b}{\epsilon_b^3}\right)\left(\frac{\rho u_o^2}{D_p}\right)\left(\frac{150}{Re_p} + 1.75\right)$$

Boundary conditions:

$$\epsilon_b D_{\mathrm{ax},i} \frac{\partial C_i}{\partial z}\Big|_{z=0} = u_{in}\left(C_i\big|_{z=0} \quad C_{i,in}\right),$$
$$\epsilon_b \lambda_{\mathrm{ax}} \frac{\partial T}{\partial z}\Big|_{z=0} = u_{in} C_T \left(T\big|_{z=0} \quad T_{in}\right),$$
$$\frac{\partial C_i}{\partial z}\Big|_{z=L} = \frac{\partial T}{\partial z}\Big|_{z=L} = 0, \qquad P\big|_{z=L} = P_{out}.$$

Solid phase

Mass balance:

$$\frac{\partial(\epsilon_c C_{c,i})}{\partial t} + \frac{1}{r_c^2}\frac{\partial}{\partial r_c}(r_c^2 J_i) = \rho_s \sum R_i$$

Energy balance:

$$\left((1 \quad \epsilon_c)\rho_s C_{p,s} + \epsilon_c C_{p,c} C_{T,c}\right)\frac{\partial T_c}{\partial t} = \frac{\lambda_s}{r_c^2}\frac{\partial}{\partial r}\left(r_c^2 \frac{\partial T_c}{\partial r_c}\right) + \rho_s \sum(\quad \Delta H_n)(R_n)$$

Dusty gas model:

$$\frac{\partial C_{c,i}}{\partial r_c} = \sum_{j=1}^{N} \frac{1}{D_{ij}^e}\left(y_k J_i \quad y_i J_k\right) + \frac{J_i}{D_{iK}^e}$$

Boundary conditions:

$$J_i\big|_{r_c=0} = 0, \qquad J_i\big|_{r_c=r_p} = k_{c,i}\left(C_{c,i}\big|_{r_c=r_p} \quad C_i\right),$$
$$\frac{\partial T_c}{\partial r_c}\Big|_{r_c=0} = 0, \qquad \lambda_s\left(\frac{\partial T_c}{\partial r_c}\right)\Big|_{r_c=r_p} = h_f\left(T_c\big|_{r_c=r_p} \quad T\right).$$

3.2 Optimal Control Formulation

The utilization of a fixed-bed reactor in CLR serves to alleviate issues associated with particle attrition, breakage,

Table 2. List of feasible reactions in the reduction and oxidation stages using Ni oxygen carriers [Han and Bollas (2016)]

Index	Reactions		
(R1)	$H_2 + NiO$	$\longrightarrow$	$Ni + H_2O$
(R2)	$CO + NiO$	$\longrightarrow$	$Ni + CO_2$
(R3)	$CH_4 + NiO$	$\longrightarrow$	$Ni + 2\,H_2 + CO$
(R4)	$CH_4 + H_2O$	$\rightleftharpoons$	$3\,H_2 + CO$
(R5)	$CO + H_2O$	$\rightleftharpoons$	$H_2 + CO_2$
(R6)	$CH_4 + CO_2$	$\rightleftharpoons$	$2\,CO + 2\,H_2$
(R7)	CH_4	$\rightleftharpoons$	$2\,H_2 + C$
(R8)	$C + H_2O$	$\rightleftharpoons$	$CO + H_2$
(R9)	$C + CO_2$	$\rightleftharpoons$	$2\,CO$
(R10)	$O_2 + 2\,Ni$	$\longrightarrow$	$2\,NiO$
(R11)	$O_2 + C$	$\longrightarrow$	CO_2
(R12)	$O_2 + 2\,C$	$\longrightarrow$	$2\,CO$
(R13)	$O_2 + 2\,CO$	$\longrightarrow$	$2\,CO_2$

and the ability to operate under high pressure. Nonetheless, this configuration introduces operational challenges primarily due to its semi-batch operation. In this system, oxygen carriers remain in the reactor, while the feed alternates to align with CLR stages and complete the cycle. These reactions are kinetically controlled and feature different reaction entalphies. Consequently, the bed temperature and the state of the oxygen carrier undergo significant changes as the feed transitions between CLR stages: OX, RED, and REF. Each CLR stage yields different gas products, resulting in downstream discontinuities. Moreover, the steam-to-methane ratio during REF is pivotal in determining the quantity of H_2 produced and in controlling carbon deposition within the reactor. To ensure a successful fixed-bed operation, a control strategy that balances the conditions in all three stages is imperative. The main challenge lies in maintaining a high H_2 production while consistently retaining sufficient heat within the reactor while meeting the constraints of fuel conversion, high N_2 concentration, and energy required for the feed gas preheating.

The general concept of this work is to design multiple fixed-bed reactors operating in parallel in order to serve a continuous product stream. One approach to tackle this challenge is to simultaneously optimize a network of CLR reactors. However, due to the high computational cost, we opted for a more practical approach, which was to optimize the operation of a single CLR reactor and then apply the optimal process to a series of identical reactors. To achieve this, we implemented an optimal control strategy aimed at determining the CLR decision variables that maximize hydrogen production while consistently meeting dynamic constraints. These decision variables include the time duration of the CLR stages: RED, REF, and OX (τ_{OX}, τ_{RED}, and τ_{REF}), feed gas temperatures, steam-to-methane ratio, and the percentage of active metal in oxygen carrier, as summarized in Table 3. It is important to note that the control profile for the feed gas is modeled using piecewise constant functions, denoted as $\mathbf{u}(\tau_i) = \mathbf{u}$, where $\mathbf{u}$ is the vector of temperature, flow, and composition of the gas stream, while τ_i is the time duration of the i-th CLR step, i.e., OX, RED, and REF. The set of control variables is summarized in the design vector, $\boldsymbol{\phi}$, shown in (1), which is constrained by upper and lower limits defined within the design space, $\boldsymbol{\Phi}$.

Table 3. Control variables for the optimal control CLR Reactor

Control variables	Notations
Feed gas temperature Steam-to-methane ratio @REF Methane-to-CO_2 ratio @RED	$\mathbf{u}_i$
Time interval of OX	τ_{OX}
Time interval of RED	τ_{RED}
Time interval of REF	τ_{REF}
Active metal content in oxygen carriers	ω

$$\boldsymbol{\phi} = [\mathbf{u}_i, \tau_{\text{OX}}, \tau_{\text{RED}}, \tau_{\text{REF}}, \omega] \in \boldsymbol{\Phi}. \tag{1}$$

3.3 Optimization Formulation

The objective function of the optimal control problem is to maximize hydrogen production during the cyclic steady-state operation of the CLR fixed bed reactor. A metric of the hydrogen production efficiency, η, is presented in Eq. (2), as the ratio of total energy carried by H_2 produced to the total energy carried by CH_4 fed into CLR reactor.

$$\eta = \frac{\int_{t_0}^{\tau_{REF}} F_{\text{out,H}_2}(t)dt}{\int_{t_0}^{t_f} F_{\text{in,CH}_4}(t)dt}, \tag{2}$$

where $F_{\text{out,H}_2}$ is the hydrogen flowrate of the exhaust stream, $F_{\text{in,CH}_4}$ is the methane flowrate of the inlet stream, t_0 and t_f are the initial time and final time of integration, with $t_f = \tau_{\text{OX}} + \tau_{\text{RED}} + \tau_{\text{REF}}$.

The optimization of the CLR fixed-bed reactor involves several constraints. The reactor must achieve a minimum methane conversion (X_{CH_4}) of 96% during both RED and REF stages as written in Eq. (3). τ_{RED} and τ_{REF} are the times required to complete RED and REF, respectively. An exit stream with high N_2 concentration is important if the process serves ammonia synthesis. Hence, in OX, the reactor must maintain an exhaust stream with a minimum N_2 mole fraction of 98%, as written in Eq. (4), where $F_{\text{out,N}_2}$ is the flowrate of the N_2 outlet streams and $F_{\text{out},T}$ is the total flowrate of the outlet streams. Since the exhaust gas is intended for feed gas preheating, it is essential that the total enthalpy carried by the exhaust gas exceeds the enthalpy required for gas preheating and steam generation, as defined in Eq. (5). $F_{\text{in},T}$ is the total flowrate of the inlet streams, c_p is the heat capacity of the inlet/oulet streams, h_{fg} is the enthalpy evaporation of the water, T_{in} and T_{out} are the temperature of inlet and outlet streams, respectively. Eq. (5) is based on assumptions in a heat exchanger: exhaust streams were cooled to 200°C, while feed streams were heated up from 25°C. Another constraint is that the maximum bed temperature, T_{bed}, at any axial location, must not exceed 1100°C, Eq. (6), to prevent the agglomeration and sintering of oxygen carriers.

$$X_{\mathrm{CH_4}}(t) = 1 - \frac{\int_{t_0}^{t_f} F_{\mathrm{out,CH_4}}(t)dt}{\int_{t_0}^{t_f} F_{\mathrm{in,CH_4}}(t)dt} \geq 96\%, \quad (3)$$

$$\beta(t) = \frac{\int_{t_0}^{\tau_{\mathrm{OX}}} F_{\mathrm{out,N_2}}(t)dt}{\int_{t_0}^{\tau_{\mathrm{OX}}} F_{\mathrm{out},T}(t)dt} \geq 98\%, \quad (4)$$

$$\gamma = \int_{t_0}^{t_f} F_{\mathrm{out},T}(t)c_{p,\mathrm{out}}(T_{\mathrm{out}}(t) - 200^{\circ}\mathrm{C})dt - \int_{t_0}^{t_f} F_{\mathrm{in},T}(t)c_{p,\mathrm{in}}(T_{\mathrm{in}}(t) - 25^{\circ}\mathrm{C})dt - \int_{t_0}^{\tau_{\mathrm{REF}}} F_{\mathrm{in,H_2O}}(t)h_{fg,\mathrm{H_2O}}dt \geq 0, \quad (5)$$

$$T_{\mathrm{bed}}(z) \leq 1100^{\circ}\mathrm{C}. \quad (6)$$

The complete optimal control problem can be formulated as shown in (7).

$$\begin{aligned} &\max_{\phi \in \mathbf{\Phi}} \eta \\ &\text{subject to:} \\ &\quad \mathbf{f}(\dot{\mathbf{x}}(t), \mathbf{x}(t), \mathbf{u}(t), \boldsymbol{\theta}, t) = 0, \\ &\quad \mathbf{f}_0(\dot{\mathbf{x}}(t_0), \mathbf{x}(t_0), \mathbf{u}(t_0), \boldsymbol{\theta}, t_0) = 0, \\ &\quad \text{Eqs.}(3) - (6), \\ &\quad \mathbf{x}^{\min} \leq \mathbf{x}(t) \leq \mathbf{x}^{\max}, \\ &\quad \mathbf{u}_i^{\min} \leq \mathbf{u}_i \leq \mathbf{u}_i^{\max}, \\ &\quad \boldsymbol{\tau}_i^{\min} \leq \boldsymbol{\tau}_i \leq \boldsymbol{\tau}_i^{\max}, \\ &\quad \omega^{\min} \leq \omega \leq \omega^{\max}. \end{aligned} \quad (7)$$

$\mathbf{f}$ is the set of differential-algebraic equations (DAEs) that describe the reactor model comprising mass, energy, and momentum balance and reaction kinetics. $\mathbf{x}$ is the vector of state variables (*i.e.*, mass, temperature, and pressure), and $\dot{\mathbf{x}}$ is the initial conditions and constraints for state $\mathbf{x}$. Cyclic steady-state conditions are typically reached after more than two cycles. Therefore, the optimization time horizon was set to at least two times the τ_{cycle}. The model was developed and solved using the commercial software gPROMS [Process Systems Enterprise (2021)].

4. RESULTS AND DISCUSSION

A case study of a small-scale Blue Hydrogen production system utilizing a CLR fixed bed reactor with a Ni-based oxygen carrier is presented. The system is designed to operate with multiple reactors, collectively achieving a hydrogen production capacity of 300 kg/day. Table 4 reports the reactor design and operating parameters, including reactor diameter, length, and operating pressure. The optimization problem defined in Eq. (7), was solved, resulting in the optimized control variables reported in Table 4. These parameters were then used in simulations to evaluate the performance of the CLR reactor system. A heat exchanger model simulates and monitors the decrease in exit gas temperature, which serves as the heat source for the preheating and steam-generating system. Figures 2 and 3 present the performance of the optimal reactor at cyclic steady state. Figure 2(d) presents the temperature of the preheating and steam generating systems.

Table 4. Fixed bed CLR reactor parameters. The top row is the common parameters, while the bottom row is the optimized parameters.

Parameters	Values		
	OX	RED	REF
Reactor length, [m]		1.5	
Reactor diameter, [m]		0.6	
Operating pressure, [bar]		1.5	
Feed volumetric flow, [NCMH]	360	36	180
CO_2-to-CH_4 ratio	–	4.0	–
Steam-to-CH_4 ratio	–	–	1.5
Feed temperature, [°C]	600	600	600
Time interval of REF, [s]	150	135	200
Active metal content in OC, [%]		5	

The optimized small-scale CLR reactor achieves a hydrogen yield efficiency of approximately 62 %, close to the performance of large-scale conventional steam reforming processes. This efficiency can be further improved with the incorporation of a hydrogen shift unit. Figure 2(a) demonstrates that a single CLR reactor produces > 65% H_2 and 20% of CO during REF. During OX, it achieved a high N_2 concentration of > 98%. The optimal control strategy maintains just enough O_2 for oxygen carrier oxidation and switches the stage to RED once the active metal has oxidized. The capability to produce both H_2 and N_2 from a single pot highlights the potential for process intensification in ammonia synthesis, a potential hydrogen carrier as reported in Hill et al. (2022) and Bagja et al. (2021). During RED, the exhaust predominantly consists of CO_2 and steam, offering opportunity for CO_2 capture simply by condensing the steam. Figure 2(a) also shows minimal methane slip in the exhaust, attributed to the consistent high methane conversion, > 97%, during both RED and REF, as depicted in Figure 2(b).

The bed temperature profile is presented in Figure 3(a). During OX, the bed temperature increased due to exothermic reactions. As the operation shifted to RED, residual heat in the bed was used for reduction reactions, while the incoming feed pushed the heat front to the end of the reactor. By the end of RED, the bed temperature was lower at the reactor front but remained similar to the early RED stage. In REF, catalytic reactions further decreased the overall bed temperature, while the feed flow pushed the heat out of the reactor. Over one CLR cycle, the highest bed temperature, approximately 960°C, was observed at roughly 85% of the reactor length by the end of RED. This bed temperature profile demonstrates how optimal control manages heat throughout the CLR cycle to achieve autothermal operation. In addition, it also shows a substantial temperature difference between the front, ranging $500 - 600^{\circ}$C, and the back of the reactor, which ranges $800 - 960^{\circ}$C.

Figure 2(c) presents the enthalpy carried by the exhaust gas of each CLR stage, along with the enthalpy needed for feed gas preheating and steam generation. The comparison shows that the energy carried by the exhaust gas, particularly during OX and RED, exceeds that required for feed gas preheating. During REF, the energy needed for the feed gas is slightly higher than the available enthalpy of the exhaust gas. However, over the course of one CLR cycle, the enthalpy carried by the exhaust gas remained higher than what was required for the feed. In

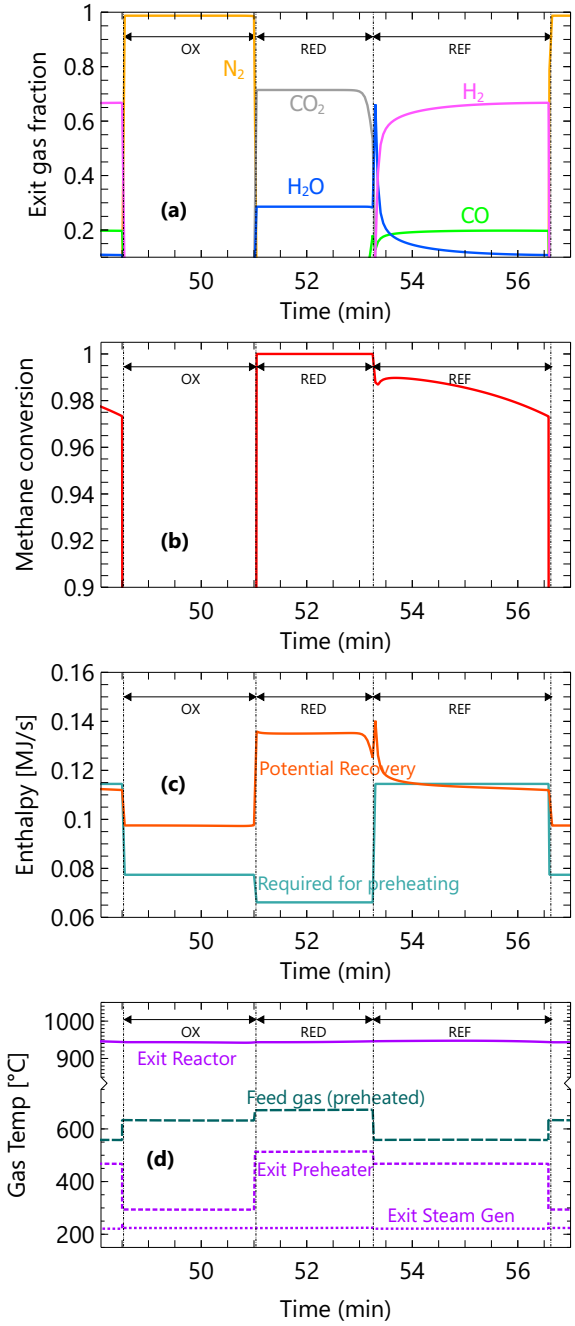

Fig. 2. Simulated CLR reactor using parameters in Table 4 during cyclic steady-state. CLR stage sequence: OX-RED-REF. (a) Exit gas fraction, (b) Methane conversion, (c) Enthalpy carried by exit gas and required for the feed gas preheating, and (d) Exit gas temperature in preheating and steam generating system (purple line); and preheated feed gas (dark blue line).

Figure 2(d) the temperature of exit gas reactor decreases to $300 - 500°C$ after passing through the preheater. This effectively preheats the feed gas to the temperature range of $550 - 650°C$. The remaining hot gas is then utilized to generate the steam required for steam-methane reforming in REF.

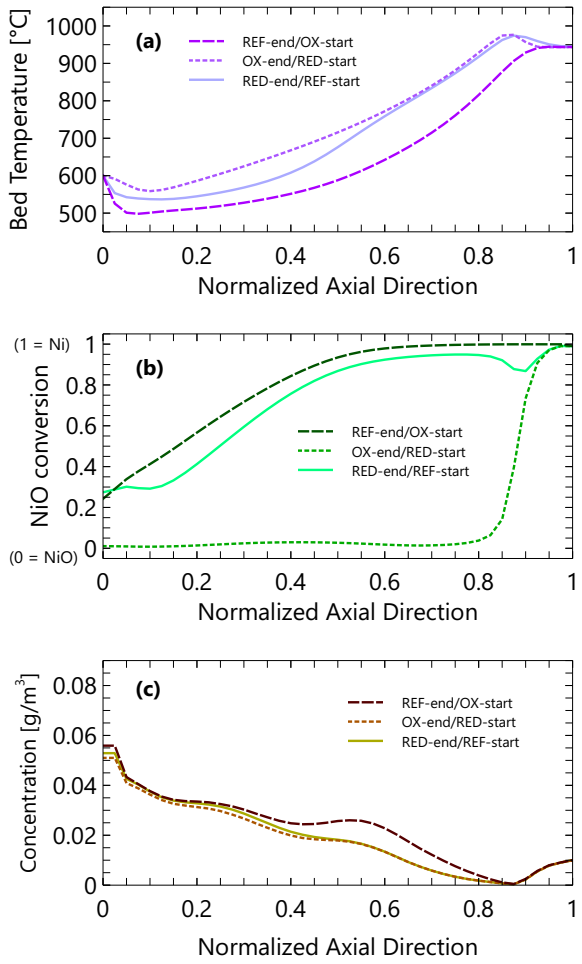

Fig. 3. Simulated CLR reactor using parameters in Table 4 during cyclic steady-state. CLR stage sequence: OX-RED-REF. (a) Bed temperature profile, (b) NiO conversion profile: scale 0 = NiO and scale 1 = Ni, and (c) profile of Carbon concentration in the reactor bed.

Figure 3(b) shows that NiO-Ni conversion occurred throughout the reactor bed, except for the region near the reactor exit, which consistently remained in the active metal form. During OX, 85-90% of the reactor bed was converted into its oxide form. During RED, the bed was converted back to its active metal state. Particularly, between 50-80% of the reactor length, where the bed temperature exceeded 700°C (Figure 3(a)) resulting in a higher NiO reduction rate. During REF, simultaneous catalytic and reduction reactions occurred and reduced the bed further to Ni. As indicated by Figure 3(c), carbon deposition within the reactor remains relatively low, below $0.08 g/m^3$. This profile was relatively consistent throughout the cycle despite the alternating feed cycles. Carbon accumulation at the first half of the reactor is attributed to the lower bed temperature in this region, as illustrated in Figure 3(a), resulting in reduced carbon oxidation during OX.

5. CONCLUSIONS

Optimal design and control scenario of a model-based CLR fixed bed reactor for Blue Hydrogen production was explored. With the optimized control strategy, the CLR reactor unit achieved hydrogen production efficiency of 62%, and was able to operate autothermally producing H_2 and N_2 from a single pot with a ratio of 0.98. The optimal control strategy maintained coke deposition minimum during the CLR process. Heat recovery was feasible to serve gas preheating and steam generation. Further optimal control for the integrated system devices, such as the addition of hydrogen shift units, need to be explored. Also, a high-temperature gradient was observed in the reactor bed which could be addressed through reverse flow operation.

ACKNOWLEDGEMENTS

This work was supported by a DIKTI-funded Fulbright Fellowship and the Pratt & Whitney Institute of Advanced Systems Engineering (P&W-IASE) of the University of Connecticut. Any opinions expressed herein are those of the author and do not represent those of the sponsor.

REFERENCES

Adanez, J., Abad, A., Garcia-Labiano, F., Gayan, P., and De Diego, L.F. (2012). Progress in chemical-looping combustion and reforming technologies. doi:10.1016/j.pecs.2011.09.001.

Arcos, J.M.M. and Santos, D.M.F. (2023). The Hydrogen Color Spectrum: Techno-Economic Analysis of the Available Technologies for Hydrogen Production. *Gases*, 3(1), 25–46. doi:10.3390/gases3010002.

Arnaiz del Pozo, C. and Cloete, S. (2022). Techno-economic assessment of blue and green ammonia as energy carriers in a low-carbon future. *Energy Conversion and Management*, 255(January), 115312. doi:10.1016/j.enconman.2022.115312. URL `https://doi.org/10.1016/j.enconman.2022.115312`.

Bagja, F., Rizqi, A., and Aziz, M. (2021). ScienceDirect Production of ammonia as potential hydrogen carrier : Review on thermochemical and electrochemical processes. *International Journal of Hydrogen Energy*, 46(27), 14455–14477. doi:10.1016/j.ijhydene.2021.01.214. URL `https://doi.org/10.1016/j.ijhydene.2021.01.214`.

Bloomberg NEF (2020). Hydrogen Economy Outlook. *Bloomberg New Energy Finance*, 12.

George, J.F., Müller, V.P., Winkler, J., and Ragwitz, M. (2022). Is blue hydrogen a bridging technology? - The limits of a CO2 price and the role of state-induced price components for green hydrogen production in Germany. *Energy Policy*, 167. doi:10.1016/j.enpol.2022.113072.

Han, L. and Bollas, G.M. (2016). Chemical-looping combustion in a reverse-flow fixed bed reactor. *Energy*, 102, 669–681. doi:10.1016/j.energy.2016.02.057. URL `http://dx.doi.org/10.1016/j.energy.2016.02.057`.

Han, L., Zhou, Z., and Bollas, G.M. (2013). Heterogeneous modeling of chemical-looping combustion. Part 1: Reactor model. *Chemical Engineering Science*, 104, 233–249. doi:10.1016/j.ces.2013.09.021. URL `http://dx.doi.org/10.1016/j.ces.2013.09.021`.

Han, L., Zhou, Z., and Bollas, G.M. (2014). Heterogeneous modeling of chemical-looping combustion. Part 2: Particle model. *Chemical Engineering Science*, 113, 116–128. doi:10.1016/j.ces.2014.03.030. URL `http://dx.doi.org/10.1016/j.ces.2014.03.030`.

Han, L., Zhou, Z., and Bollas, G.M. (2016a). Model-Based Analysis of Chemical-Looping Combustion Experiments. Part I: Structural Identifiability of Kinetic Models for NiO Reduction. *AIChE Journal*, 62(7), 2419–2431. doi:10.1002/aic.

Han, L., Zhou, Z., and Bollas, G.M. (2016b). Model-based analysis of chemical-looping combustion experiments. Part II: Optimal design of CH4-NiO reduction experiments. *AIChE Journal*, 62(7), 2432–2446. doi:10.1002/aic.15242.

Hill, C., Robbins, R., Furler, P., Ackermann, S., and Scheffe, J. (2022). Kinetic investigation of solar chemical looping reforming of methane over Ni-CeO2 at low temperature. *Sustainable Energy and Fuels*, 7(2), 574–584. doi:10.1039/d2se01452a.

Howarth, R.W. and Jacobson, M.Z. (2022). Reply to comment on "How Green is Blue Hydrogen?". *Energy Science and Engineering*, 10(7), 1955–1960. doi:10.1002/ese3.1154.

IEA (2020). Energy Technology Perspectives 2020. Technical report. doi:10.1787/ab43a9a5-en.

IEA (2023). Towards hydrogen definitions based on their emissions intensity. Technical report. URL `www.iea.org`.

NASA (2023). Global Climate Change: Global Temperature.

Nazir, S.M., Cloete, J.H., Cloete, S., and Amini, S. (2021). Pathways to low-cost clean hydrogen production with gas switching reforming. *International Journal of Hydrogen Energy*, 46(38), 20142–20158. doi:10.1016/j.ijhydene.2020.01.234.

Newborough, M. and Cooley, G. (2020). Developments in the global hydrogen market: The spectrum of hydrogen colours. *Fuel Cells Bulletin*, 2020(11), 16–22. doi:10.1016/S1464-2859(20)30546-0.

Nordness, O., Han, L., Zhou, Z., and Bollas, G.M. (2016). High-Pressure Chemical-Looping of Methane and Synthesis Gas with Ni and Cu Oxygen Carriers. *Energy and Fuels*, 30(1), 504–514. doi:10.1021/acs.energyfuels.5b01986.

Process Systems Enterprise (2021). gPROMS. URL `www.psenterprise.com/products/gproms`.

UN Climate Change (2023). Key aspects of the Paris Agreement.

Zhou, Z., Han, L., and Bollas, G.M. (2013). Model-based analysis of bench-scale fixed-bed units for chemical-looping combustion. *Chemical Engineering Journal*, 233, 331–348. doi:10.1016/j.cej.2013.08.025. URL `http://dx.doi.org/10.1016/j.cej.2013.08.025`.

Zhou, Z., Han, L., and Bollas, G.M. (2014). Kinetics of NiO reduction by H2 and Ni oxidation at conditions relevant to chemical-looping combustion and reforming. In *International Journal of Hydrogen Energy*, volume 39, 8535–8556. Elsevier Ltd. doi:10.1016/j.ijhydene.2014.03.161.